



Supplement of

Uncertainty and retrieval sensitivity in TROPOMI-based methane inversions over the North Slope of Alaska

Rebecca H. Ward et al.

Correspondence to: Rebecca H. Ward (rebecca.ward@fmi.fi)

The copyright of individual parts of the supplement might differ from the article licence.

Supplement

S1: Derivation of perturbed XCH_4

We convert our modelled CH_4 for each retrieval into a column mole fraction ($\text{XCH}_4^{\text{model}}$) for each time index, t , as follows,

$$\text{XCH}_4^{\text{model}}|_t = \sum_1^n p_i \left[A_i \cdot \text{CH}_{4,i}^{\text{model}} + (1 - A_i) \cdot \text{CH}_{4,i}^{\text{prior}} \right], \quad (\text{S1})$$

where p_i is the pressure weight, A_i is the averaging kernel, $\text{CH}_{4,i}^{\text{model}}$ is the modelled CH_4 mole fraction and $\text{CH}_{4,i}^{\text{prior}}$ is the a priori profile at each level i from the surface to the top of the atmosphere.

We know $\text{CH}_{4,i}^{\text{prior}}$, A_i and p_i , so the second term can be subtracted from Eq. (S1) and we derive a perturbed column averaged mole fraction, $\text{XCH}_{4,\text{pert}}^{\text{model}}|_t$, as follows,

$$\text{XCH}_4^{\text{model}}|_t - \sum_1^n p_i (1 - A_i) \cdot \text{CH}_{4,i}^{\text{prior}} = \sum_1^n p_i \cdot A_i \cdot \text{CH}_{4,i}^{\text{model}} \quad (\text{S2})$$

We replace the levels above max level to be equal to the prior value as described above, such that,

$$\text{XCH}_4^{\text{model}}|_t - \sum_1^n p_i (1 - A_i) \cdot \text{CH}_{4,i}^{\text{prior}} = \sum_1^{\text{maxlev}} p_i \cdot A_i \cdot \text{CH}_{4,i}^{\text{model}} + \sum_{\text{maxlev}+1}^n p_i \cdot A_i \cdot \text{CH}_{4,i}^{\text{prior}} \quad (\text{S3})$$

Rearranging,

$$\text{XCH}_4^{\text{model}}|_t - \sum_1^n p_i (1 - A_i) \cdot \text{CH}_{4,i}^{\text{prior}} - \sum_{\text{maxlev}+1}^n p_i \cdot A_i \cdot \text{CH}_{4,i}^{\text{prior}} = \sum_1^{\text{maxlev}} p_i \cdot A_i \cdot \text{CH}_{4,i}^{\text{model}} \quad (\text{S4})$$

Taking the left hand side,

$$\text{XCH}_4^{\text{model}}|_t - \left(\sum_1^n p_i \cdot \text{CH}_{4,i}^{\text{prior}} - \sum_1^n p_i \cdot A_i \cdot \text{CH}_{4,i}^{\text{prior}} + \sum_{\text{maxlev}+1}^n p_i \cdot A_i \cdot \text{CH}_{4,i}^{\text{prior}} \right) \quad (\text{S5})$$

$$\begin{aligned} \text{XCH}_4^{\text{model}}|_t - \left(\sum_1^{\text{maxlev}} p_i \cdot \text{CH}_{4,i}^{\text{prior}} + \sum_{\text{maxlev}+1}^n p_i \cdot \text{CH}_{4,i}^{\text{prior}} - \sum_1^{\text{maxlev}} p_i \cdot A_i \cdot \text{CH}_{4,i}^{\text{prior}} - \right. \\ \left. \sum_{\text{maxlev}+1}^n p_i \cdot A_i \cdot \text{CH}_{4,i}^{\text{prior}} + \sum_{\text{maxlev}+1}^n p_i \cdot A_i \cdot \text{CH}_{4,i}^{\text{prior}} \right) \quad (\text{S6}) \end{aligned}$$

Cancelling out and simplifying gives us $\text{XCH}_{4,\text{pert}}^{\text{model}}|_t$,

$$\text{XCH}_{4,\text{pert}}^{\text{model}}|_t = \text{XCH}_4^{\text{model}}|_t - \sum_1^{\text{maxlev}} p_i (1 - A_i) \cdot \text{CH}_{4,i}^{\text{prior}} - \sum_{\text{maxlev}+1}^n p_i \cdot \text{CH}_{4,i}^{\text{prior}} \quad (\text{S7})$$

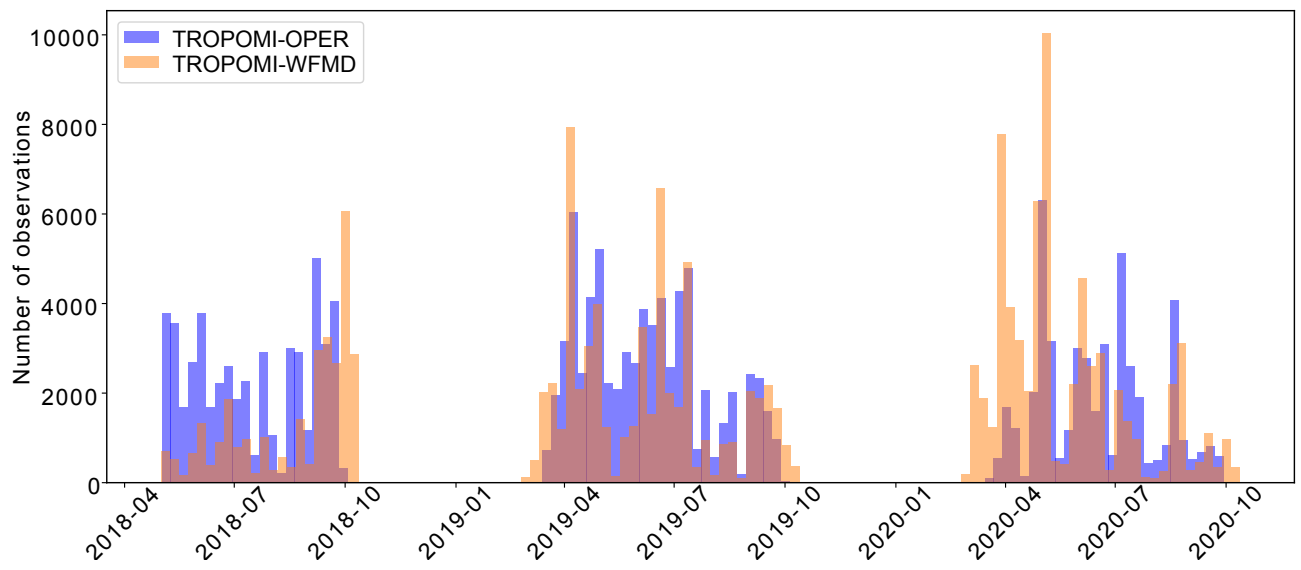


Figure S1: Number of regridded observations from TROPOMI-OPER (blue) and TROPOMI-WFMD (orange) for 2018-2020 the North Slope of Alaska, after regridding to $0.234^\circ \times 0.352^\circ$ spatial and one hourly temporal resolution.

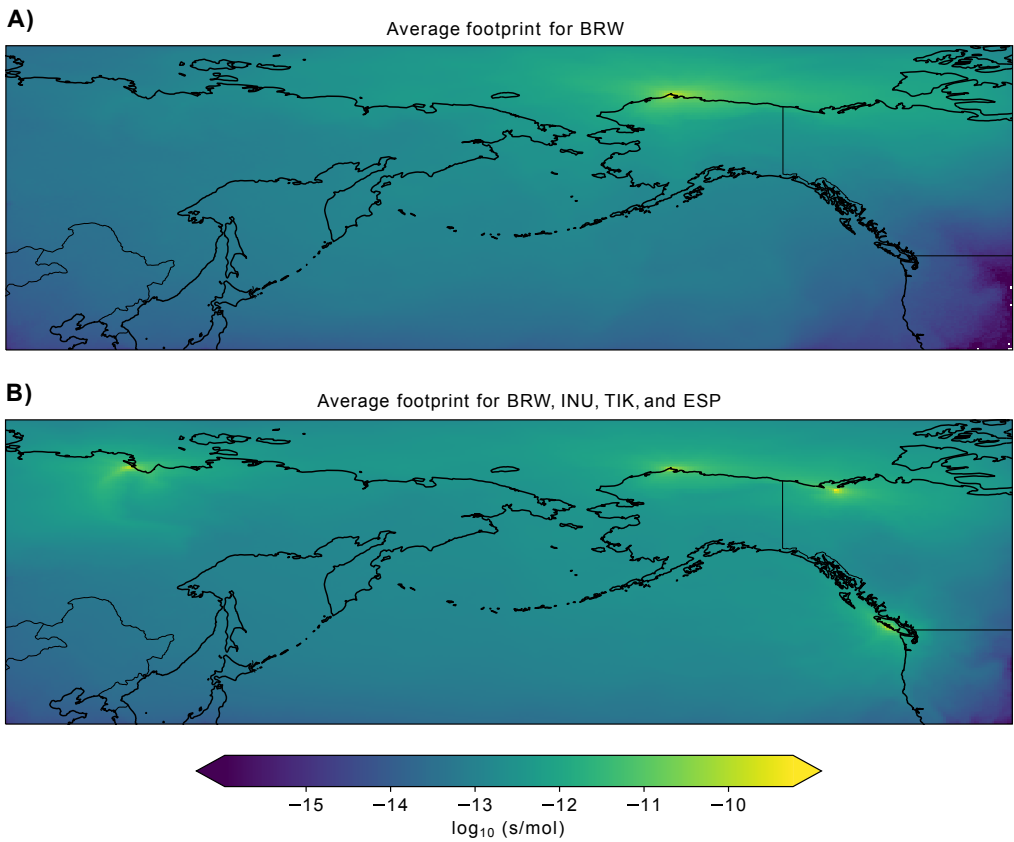


Figure S2: Average footprints in 2019 for A) BRW only B) BRW, INU, TIK and ESP, over the Alaska domain.

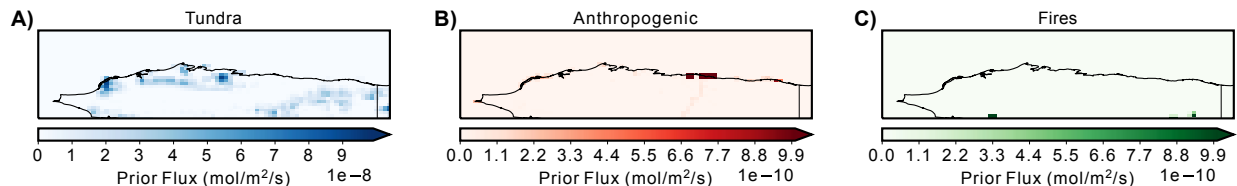


Figure S3: Prior emissions maps for the three major source sectors over the North Slope of Alaska for August 2019 for the A) Late-season Zona tundra emissions B) anthropogenic emissions and C) fire emissions. Note the different orders of magnitude of each scale.

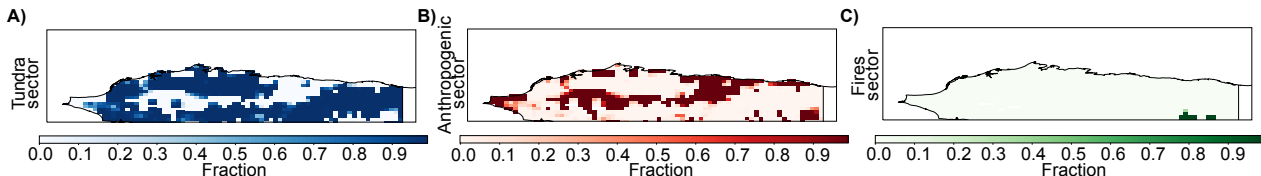


Figure S4: The fraction of emissions from each of the three major source sectors over the North Slope of Alaska for A) tundra, B) anthropogenic and C) fires. Shown here for June 2019.

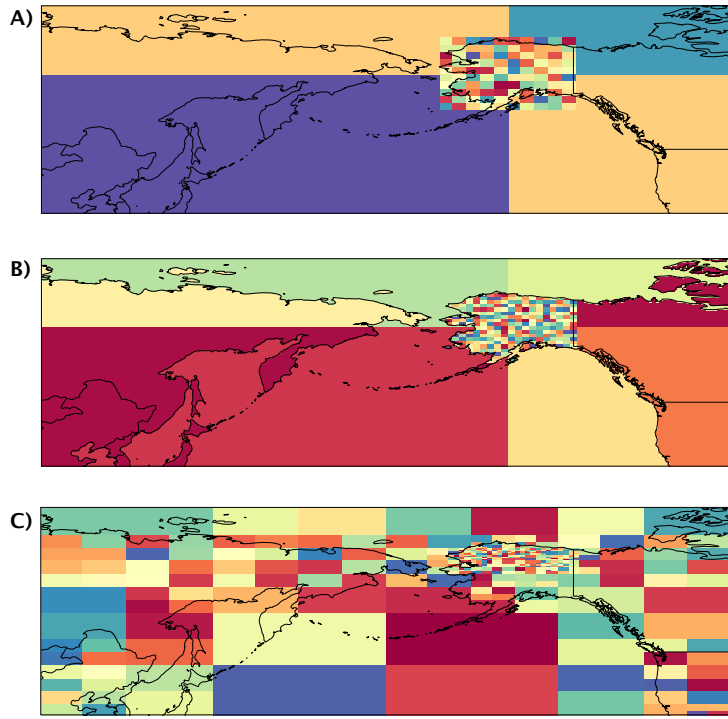


Figure S5: Grid cell aggregations for A) 104 cells, B) 297 cells and C) 421 cells in the Alaska domain. The grid colors have no meaning, except to show the size of each cell.

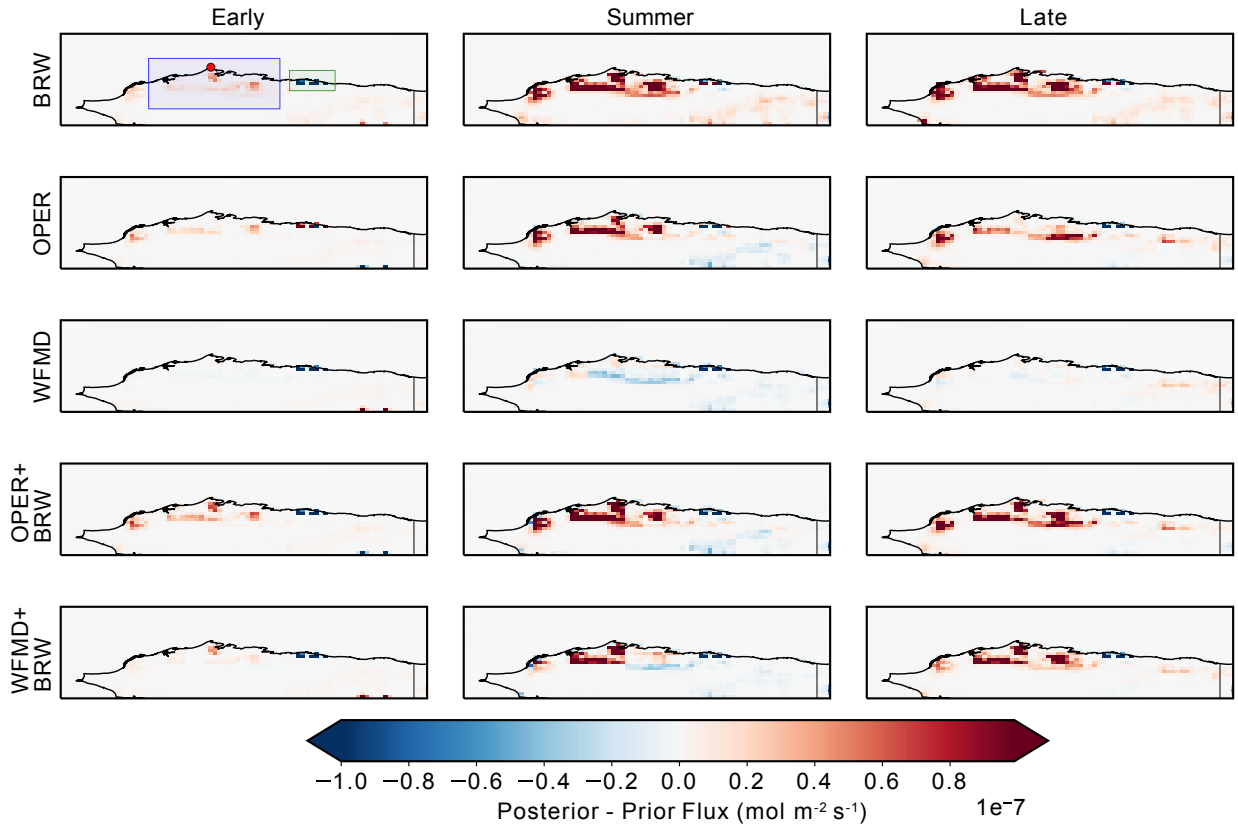


Figure S6: Average seasonal difference maps (posterior emissions - prior emissions) for each of the BRW, TROPOMI-OPER and TROPOMI-WFMD inversions for 2018–2020. Blue colours indicate a decrease in emissions from the prior to posterior, and red colours indicate an increase in emissions from prior to posterior. In the top right panel, the BRW site is marked with a red circle, a key tundra region with a blue rectangle, and the Prudhoe Bay oil fields with a green square.

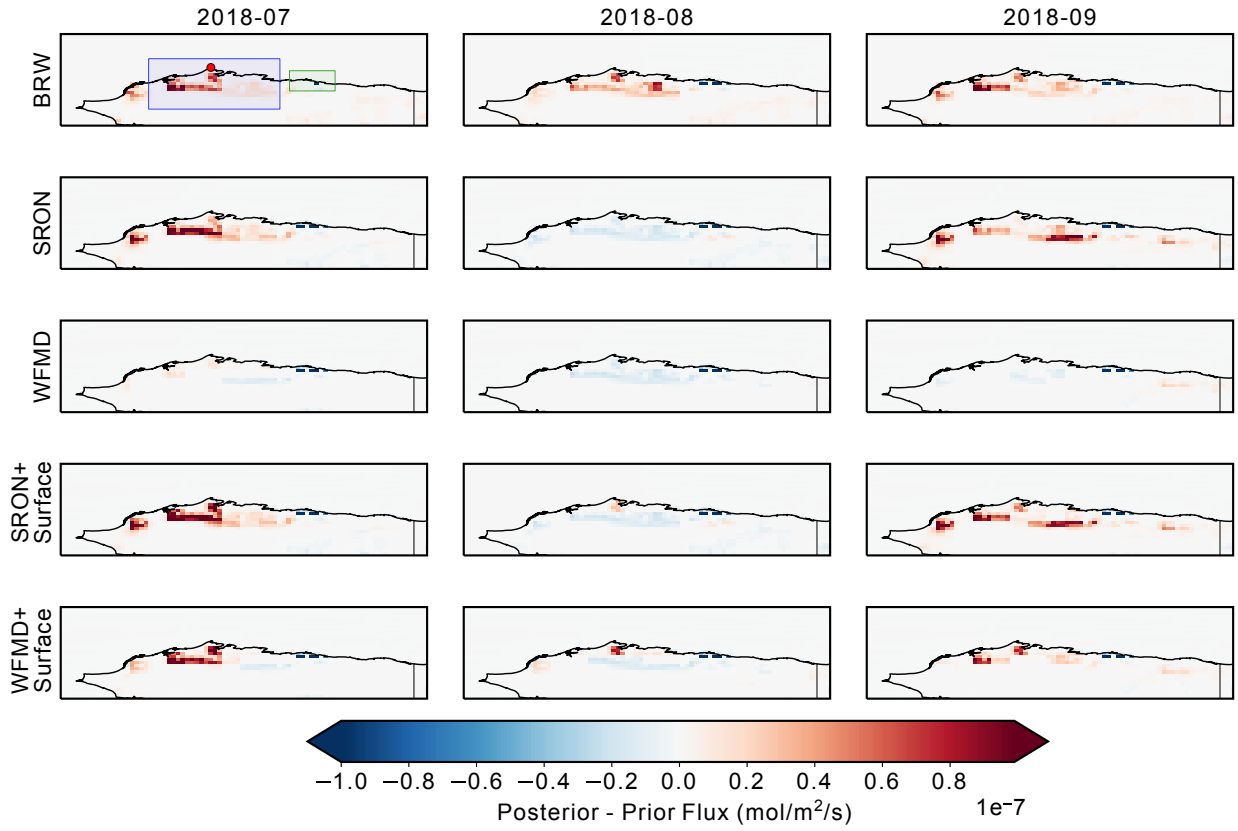


Figure S7: July, August, and September 2018 difference maps (posterior emissions - prior emissions) for each of the BRW, TROPOMI-OPER and TROPOMI-WFMD inversions. Blue colours indicate a decrease in emissions from the prior to posterior, and red colours indicate an increase in emissions from prior to posterior. In the top right panel, the BRW site is marked with a red circle, a key tundra region with a blue rectangle, and the Prudhoe Bay oil fields with a green square.

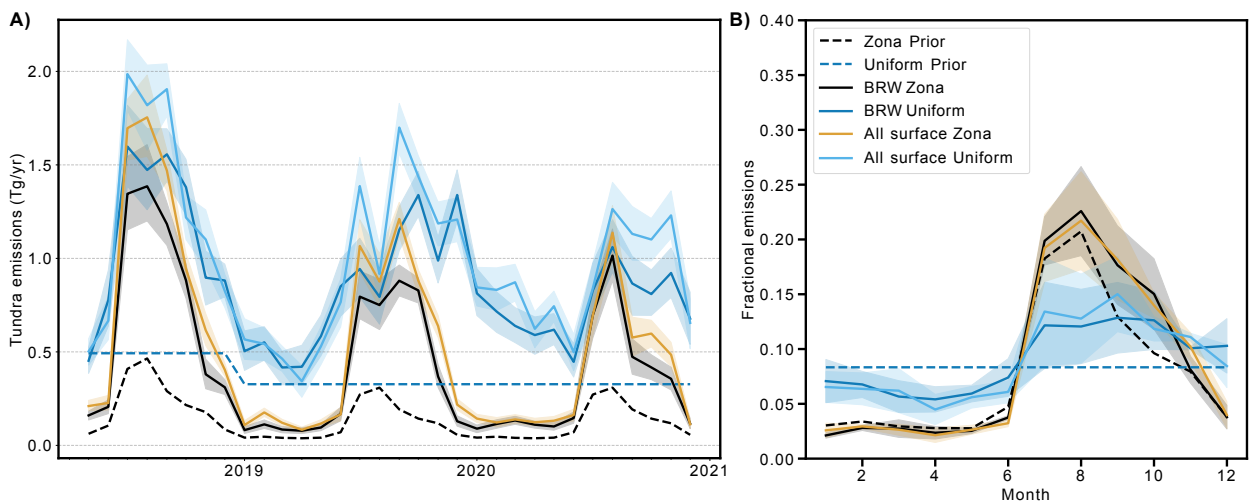


Figure S8: Uniform prior sensitivity test for the BRW-only and surface inversions. Derived emissions are shown in A) and the average seasonal profiles are shown in B). Prior emissions are shown by dashed lines.

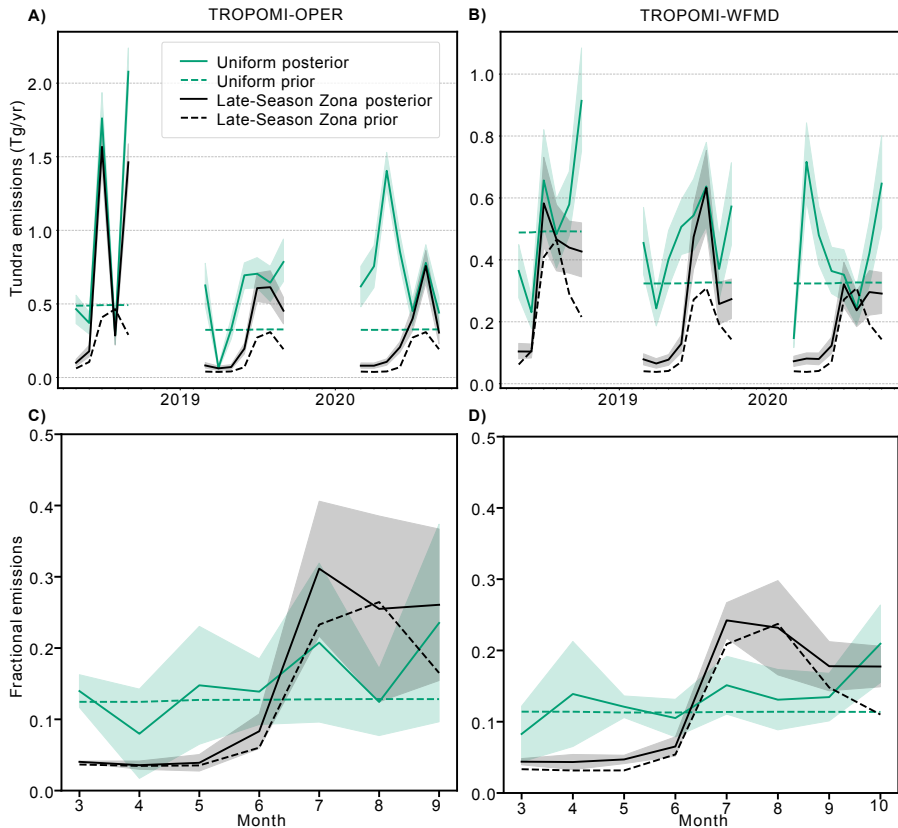


Figure S9: Uniform prior sensitivity tests for the satellite inversions. Derived tundra emissions for TROPOMI-OPER and TROPOMI-WFMD shown in A) and B), respectively. Corresponding average seasonal profiles are shown in D) and E), respectively. Tundra emissions derived with the Uniform prior are in green. Tundra emissions derived with the Late-Season Zona prior (from the main inversion) are in black.

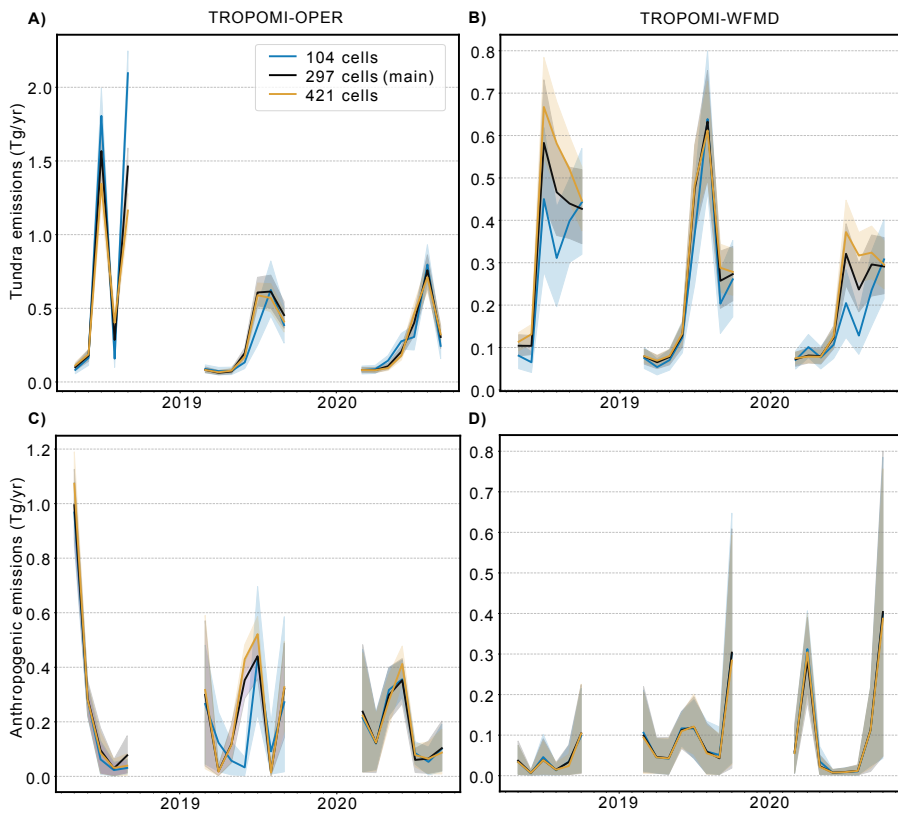


Figure S10: Grid aggregation sensitivity tests for tundra emissions using A) TROPOMI-OPER and B) TROPOMI-WFMD and for anthropogenic emissions using C) TROPOMI-OPER and D) TROPOMI-WFMD. Emissions derived using 104 aggregated grid cells are in blue, 297 cells (as in the main inversion) are in black and 421 cells are in orange.

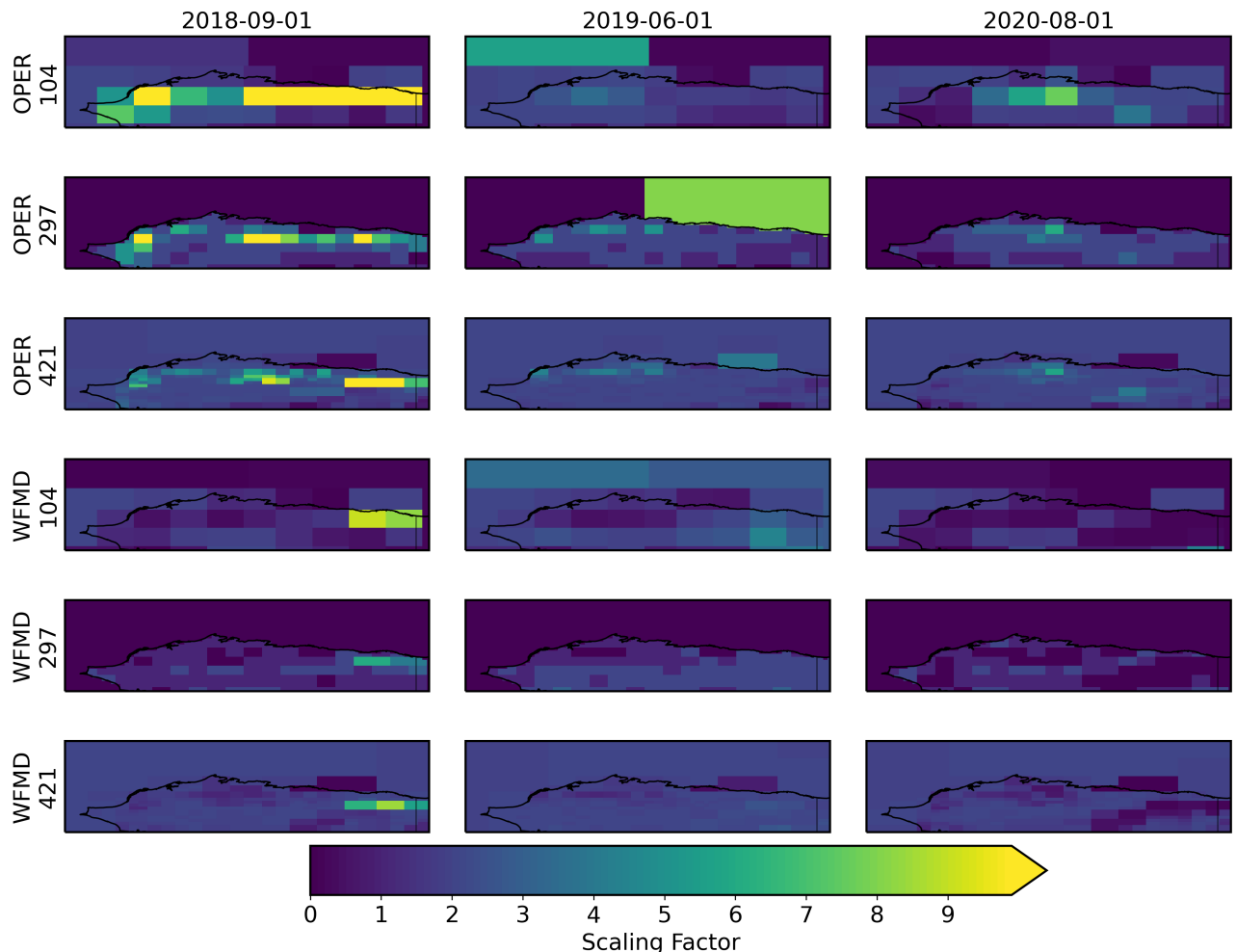


Figure S11: Spatial scaling factors over the NSA for the grid cell aggregations sensitivity test. Scaling factors are shown for selected months which show significant changes in the total monthly tundra or anthropogenic emissions.

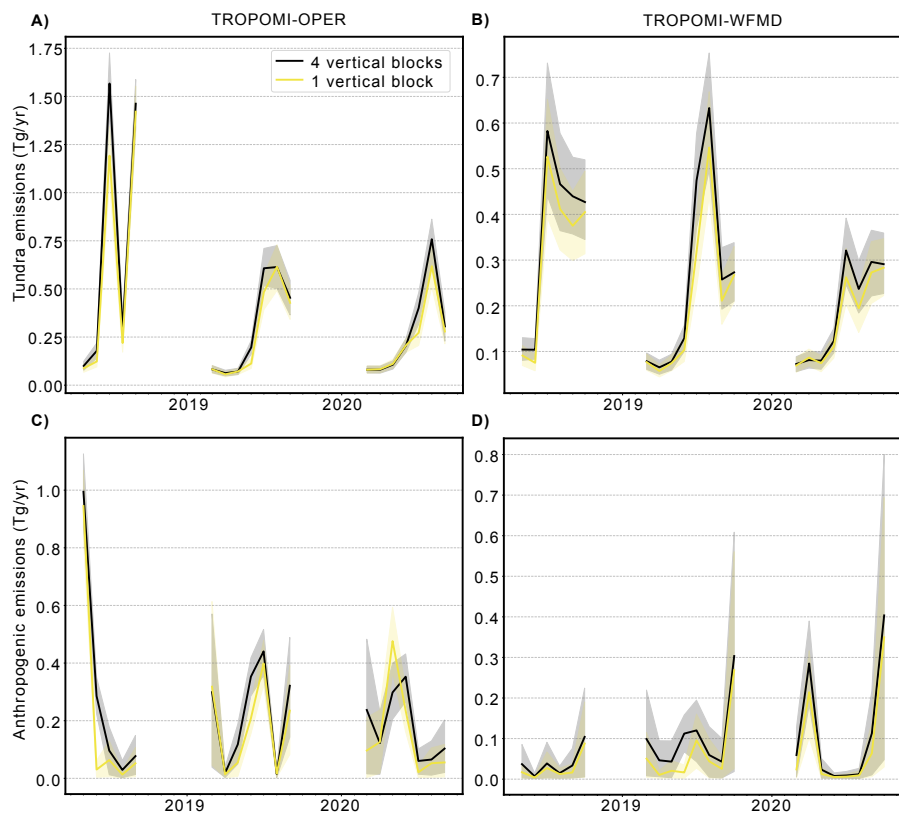


Figure S12: Vertical boundary condition sensitivity test for tundra emissions using A) TROPOMI-OPER and B) TROPOMI-WFMD and for anthropogenic emissions using C) TROPOMI-OPER and D) TROPOMI-WFMD. Emissions derived with 4 vertical boundary condition blocks (as in the main inversion) are shown in black. Tundra emissions derived with only 1 vertical boundary condition block are shown in yellow.

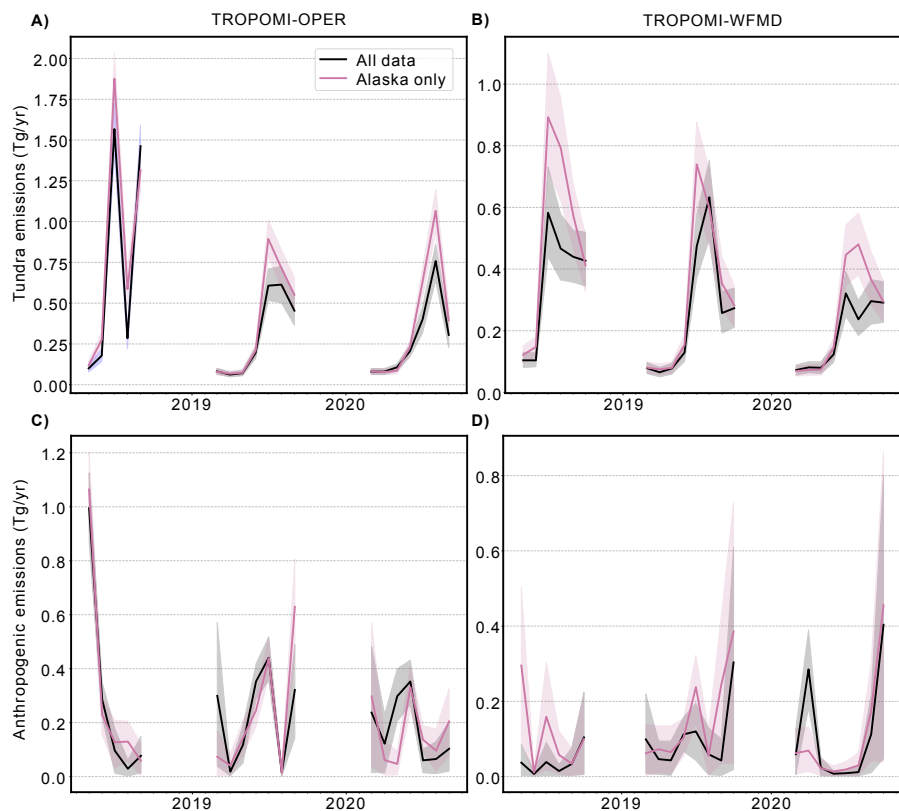


Figure S13: Alaska observations only sensitivity test for tundra emissions using A) TROPOMI-OPER and B) TROPOMI-WFMD and for anthropogenic emissions using C) TROPOMI-OPER and D) TROPOMI-WFMD. Emissions derived with observations across the whole domain are in black. Emissions derived with only observations from Alaska are in pink.

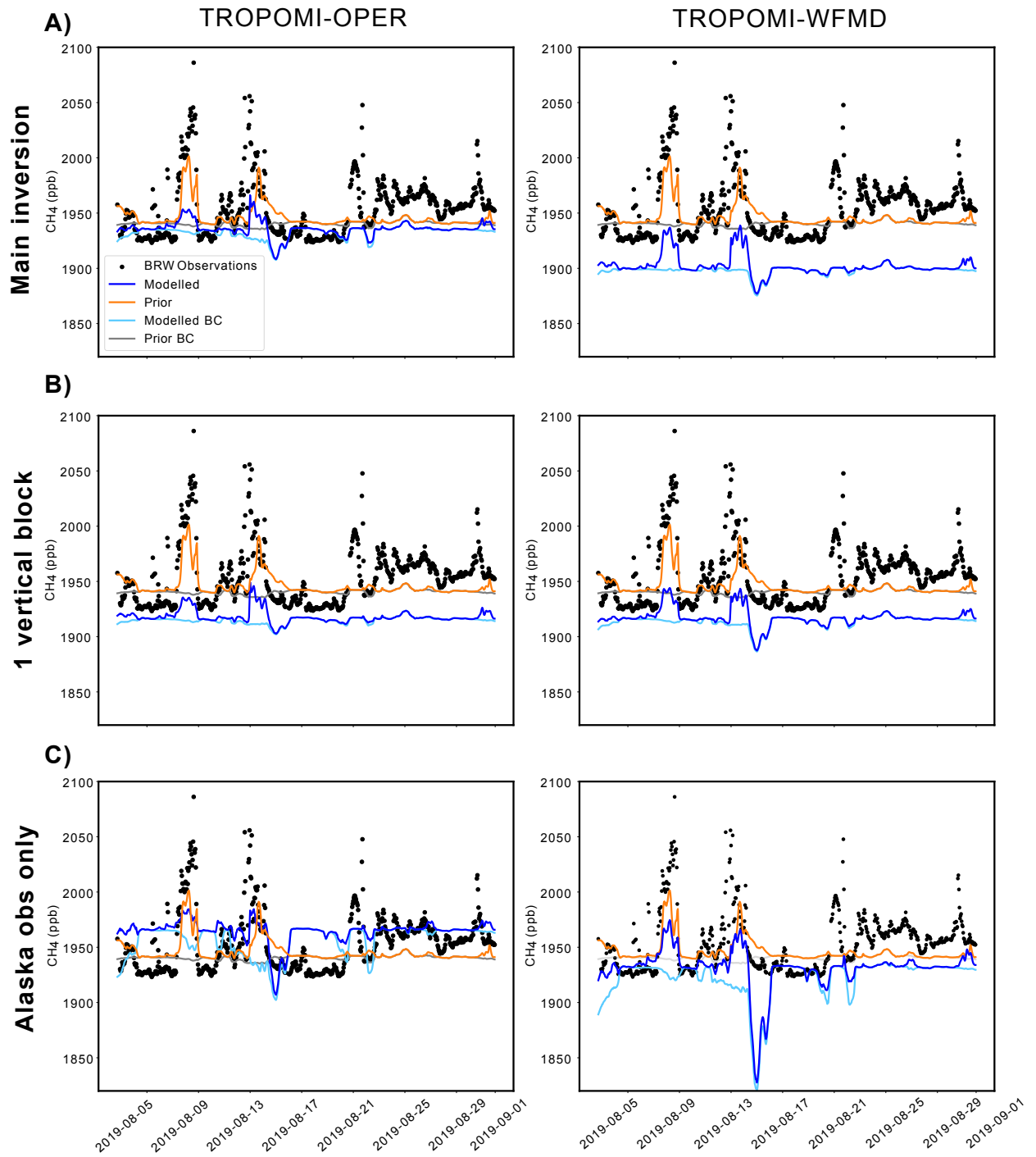


Figure S14: Forward modelled mole fractions at BRW for August 2019. The forward model using TROPOMI derived emissions and boundary condition scaling factors are shown in dark blue for the main inversion (A) and for two sensitivity tests one vertical block (B) and Alaska observations only (C). TROPOMI-OPER is in the left hand column and TROPOMI-WFMD is in the right hand column). The prior forward model is shown in light blue and the BRW observed mole fractions are shown by black dots.

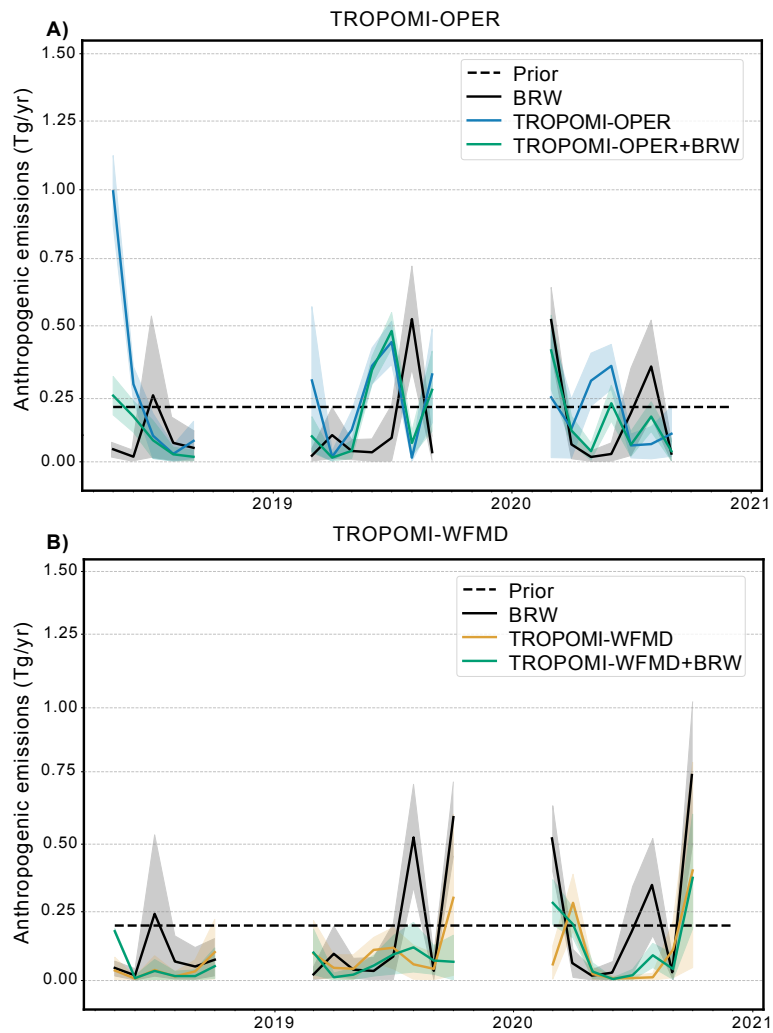


Figure S15: Combined TROPOMI+BRW inversions. A) and B) show the anthropogenic sector emissions for the TROPOMI-OPER+BRW and TROPOMI-WFMD+BRW inversions, respectively

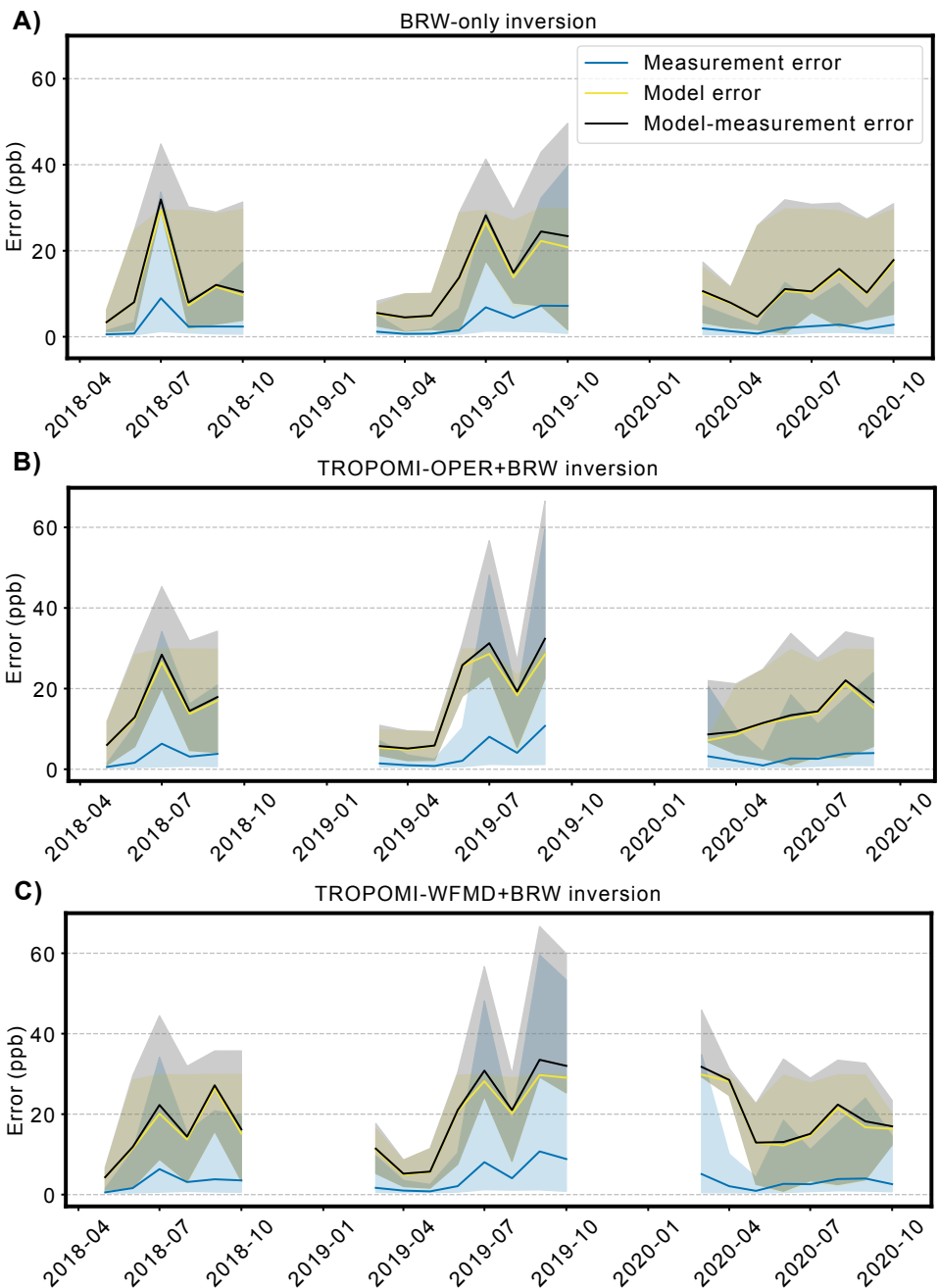


Figure S16: Monthly averaged BRW inversion uncertainties for A) the BRW-only inversion B) the TROPOMI-OPER+BRW inversion and C) the TROPOMI-SRON+BRW inversion. The measurement error (blue) is the uncertainty provided by the retrieval/measurements. The model error (yellow), is optimised throughout the inversion. The model-measurement error (black), is the measurement and model error combined in quadrature. The shaded bands show the 95% CI (2.5–97.5%) of each of the errors.

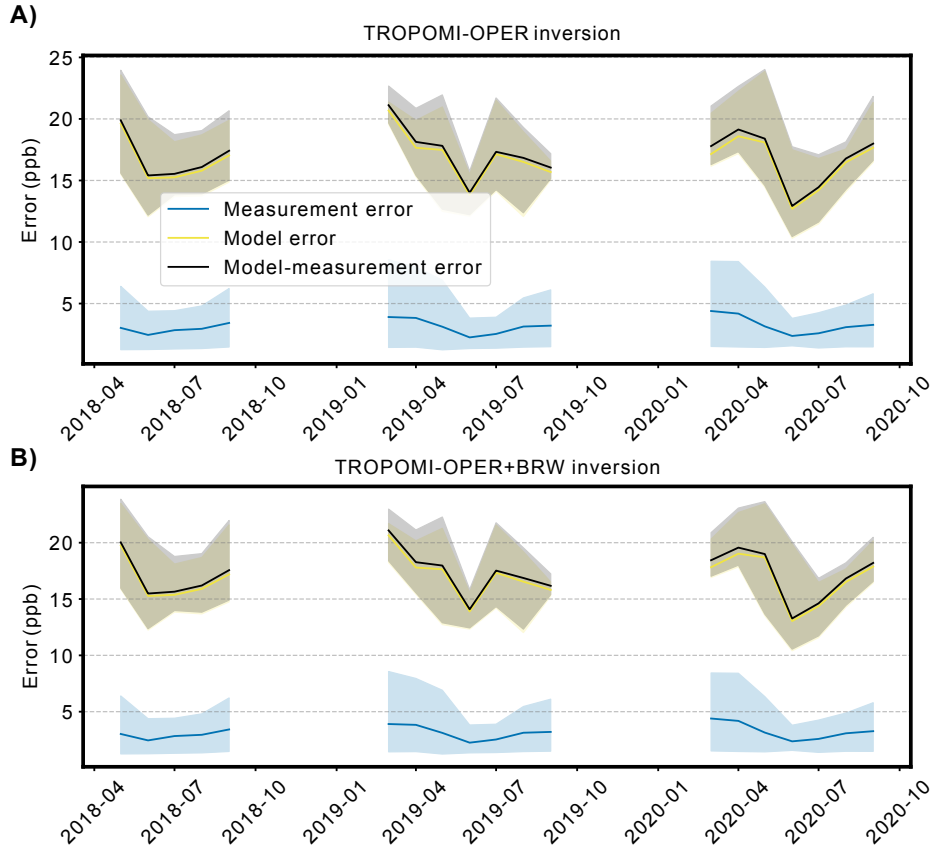


Figure S17: Monthly averaged TROPOMI-OPER uncertainties for A) the TROPOMI-OPER only inversion and B) the TROPOMI-OPER+BRW inversion. In B) the top panel is the error for TROPOMI-OPER and the bottom panel is for BRW. The measurement error (blue) is the uncertainty provided by the retrieval/measurements. The model error (yellow), is optimised throughout the inversion. The model-measurement error (black), is the measurement and model error combined in quadrature. The shaded bands show the 95% CI (2.5–97.5%) of each of the errors.

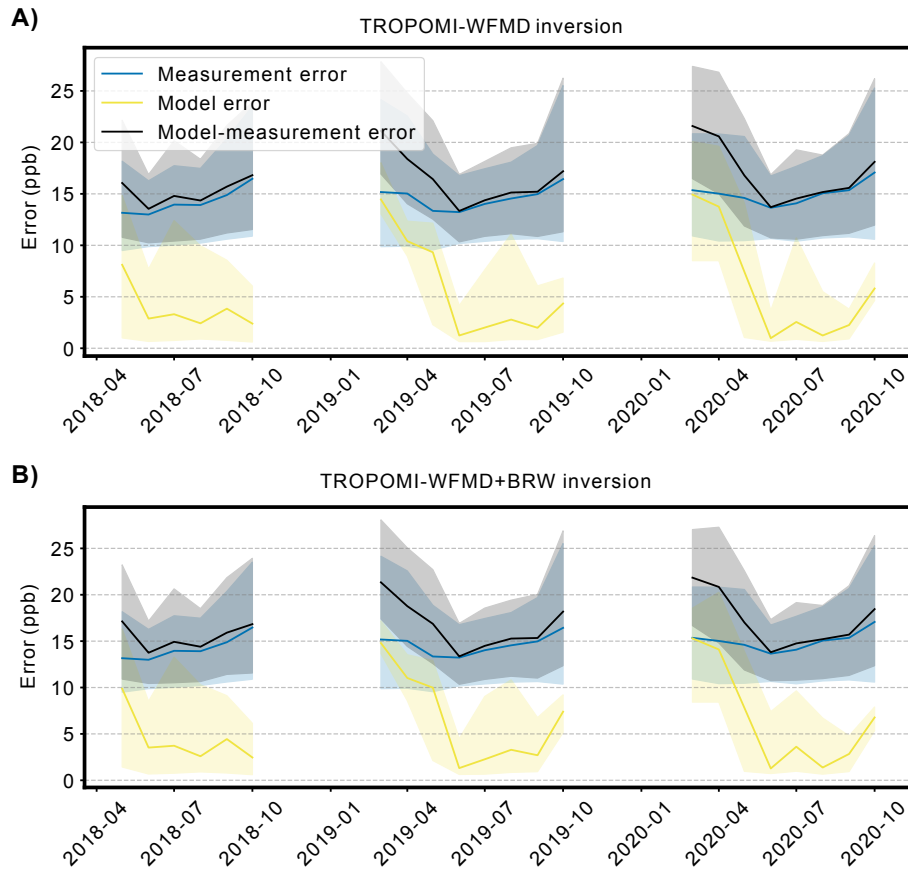


Figure S18: Monthly averaged TROPOMI-WFMD uncertainties for A) the TROPOMI-WFMD only inversion and B) the TROPOMI-WFMD+BRW inversion. In B) the top panel is the error for TROPOMI-WFMD and the bottom panel is for BRW. The measurement error (blue) is the uncertainty provided by the retrieval/measurements. The model error (yellow), is optimised throughout the inversion. The model-measurement error (black), is the measurement and model error combined in quadrature. The shaded bands show the 95% CI (2.5–97.5%) of each of the errors.

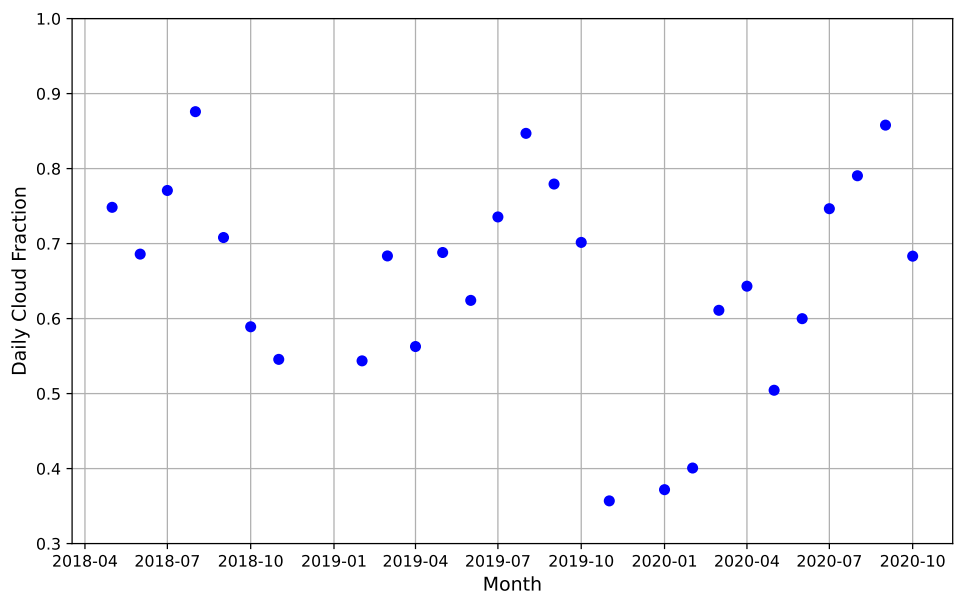


Figure S19: Average cloud fraction during daylight hours (defined as when solar zenith angle is less than 85°) over the North Slope of Alaska for each month of the study period. Calculated using the VIIRS/SNPP Cloud Properties Level 3 monthly dataset [1].

Supplementary Tables

Inversion name	Tundra emissions	Anthropogenic emissions
BRW only (this study)	0.39 (0.06, 0.98)	0.15 (0.00, 0.56)
BRW only (Ward et al., 2024)	0.50 (0.05, 1.25)	0.09 (0.00, 0.46)
All-surface (this study)	0.47 (0.07, 1.21)	0.24 (0.00, 0.76)
TROPOMI-OPER main	0.29 (0.05, 0.73)	0.20 (0.00, 0.45)
TROPOMI-OPER Uniform prior	0.65 (0.05, 1.37)	0.17 (0.00, 0.49)
TROPOMI-OPER 104 cells	0.26 (0.05, 0.78)	0.18 (0.00, 0.45)
TROPOMI-OPER 421 cells	0.28 (0.05, 0.69)	0.21 (0.00, 0.52)
TROPOMI-OPER 1 vertical block	0.25 (0.04, 0.64)	0.16 (0.00, 0.47)
TROPOMI-OPER Alaska obs only	0.37 (0.05, 1.03)	0.20 (0.00, 0.59)
TROPOMI-OPER+BRW	0.39 (0.07, 1.08)	0.17 (0.00, 0.48)
TROPOMI-WFMD main	0.21 (0.05, 0.60)	0.07 (0.00, 0.26)
TROPOMI-WFMD Uniform prior	0.42 (0.12, 0.71)	0.07 (0.00, 0.28)
TROPOMI-WFMD 104 cells	0.18 (0.03, 0.59)	0.08 (0.00, 0.29)
TROPOMI-WFMD 421 cells	0.22 (0.05, 0.59)	0.07 (0.00, 0.28)
TROPOMI-WFMD 1 vertical block	0.18 (0.04, 0.52)	0.04 (0.00, 0.19)
TROPOMI-WFMD Alaska obs only	0.27 (0.05, 0.72)	0.09 (0.00, 0.27)
TROPOMI-WFMD+BRW	0.31 (0.05, 0.83)	0.08 (0.00, 0.27)

Table S1: Average emissions for March-September 2019 and 2020 in Tg yr^{-1} for all inversions carried out in this study. The emissions are shown separately for the tundra and anthropogenic sectors. Values in brackets are the lower and upper 95% confidence interval calculated from all MCMC samples in the time period.

References

[1] VIIRS Atmosphere Science Team SSEC University Of Wisconsin-Madison: VIIRS/SNPP Cloud Properties Level 3 monthly, 1x1 degree grid [Dataset], https://doi.org/10.5067/VIIRS/CLDPROP_M3_VIIRS_SNPP.011, 2019.